Progress In Electromagnetics Research, Vol. 116, 333–346, 2011

BALANCED SINGLE- AND DUAL-BAND BPFS USING RING RESONATORS

C.-H. Lee

Graduate Institute of Communications Engineering
National Changhua University of Education
1 Jin-De Road, Changhua 500, Taiwan, R.O.C.

C.-I. G. Hsu

Department of Electrical Engineering
National Yunlin University of Science and Technology
123 University Road, Section 3, Douliou, Yunlin 640, Taiwan, R.O.C.

H.-H. Chen and Y.-S. Lin

Department of Electronic Engineering
National Changhua University of Education
1 Jin-De Road, Changhua 500, Taiwan, R.O.C.

Abstract—This paper presents new balanced single- and dual-band bandpass filters (BPFs), both of which are constructed using two ring resonators. For each BPF, open-circuited stubs are added to one of the two resonators so that the transmitted common-mode (CM) signals can be attenuated, and source-load coupling is established so that two transmission zeros are generated near the edges of each desired differential-mode (DM) passband to sharpen the passband selectivity. The measurement agrees well with the simulation. For the single-band BPF, the measured minimum DM insertion loss is 1.4 dB in the DM passband, in which the CM suppression is larger than 41.6 dB. For the dual-band BPF, the minimum DM insertion losses are 1 and 1.35 dB in the first and second passbands, respectively, in which the CM rejections are larger than 29 and 22 dB.

Received 30 March 2011, Accepted 4 May 2011, Scheduled 9 May 2011
Corresponding author: Ching-Her Lee (iecher@cc.ncue.edu.tw).

1. INTRODUCTION

In the green-energy era, energy saving is one of the main themes of study for researchers and engineers in many disciplines. To better achieve this goal, electronic devices tend to be designed to operate at lower voltages. However, electronic devices operating at lower voltages are more vulnerable to interference from noises than at higher voltages, and hence specifications in noise immunity for most electronic devices nowadays are more stringent than ever before. Balance circuits (also known as differential circuits), in comparison with their single-ended counterparts, provide the advantage of smaller noise coupling with nearby devices [1]. This is one of the reasons why balanced topology is widely adopted in integrated-circuit (IC) design.

In a wireless-communication system, BPFs play a very important role. If the surrounding blocks are of balanced type, the BPFs in the frontend of an RF system must be also implemented in balanced configuration. In the past few years, balanced BPFs have received increasing attention [2–12]. These balanced BPFs have been constructed using coupled-line structures [2, 3], branch-line structures [4, 5], and, for the most part, multi-section resonators [6–12]. Each of these multi-section resonators does not form a closed loop and hence can be referred to as an open-loop resonator. In the literature, there have been a great many single-ended BPFs that are composed of open-loop resonators [13–17]. Similarly, closed-loop resonators, alternatively called ring resonators, have been widely employed to build single-ended BPFs as well [18–25]. Although open-loop resonators have also been frequently used to construct balanced BPFs, from single-band [6, 7] to dual-band ones [8–12], so far closed-loop resonators have not yet, however. Hence, the purpose of this paper is to show that closed-loop resonators can also be employed to design new balanced BPFs in a clever manner.

In this paper, we propose two balanced BPFs, one single-banded and the other dual-banded. The single-band BPF consists of two uniform-impedance square-ring resonators, and the dual-band one comprises two stepped-impedance rectangular-ring resonators. Both BPFs are arranged in symmetric fashion so that the resonant voltage distributions on the resonators can be classified into odd and even modes, odd and even relative to the structure's plane of symmetry (POS), respectively. The odd modes can support differential-mode (DM) transmission, whereas the even modes, common-mode (CM) transmission. For both BPFs, the CM transmission is effectively suppressed by separating the even-mode resonant frequencies, which is achieved by loading one of the ring resonators with open-circuited

stubs. The measured and simulated results agree reasonably well with each other and show very good DM and CM responses.

2. DESIGN OF BALANCED SINGLE-BAND BPF

2.1. BPF Configuration and Design

Figure 1(a) shows the geometry of the proposed balanced single-band BPF consisting of two square-ring resonators. For convenience, refer to the resonator on the left side as Resonator 1, and the one on the right side as Resonator 2. Each of the square-ring resonators is parallel coupled from the upper and lower sides of the resonator, respectively, to a horizontal microstrip above and below. These horizontal microstrip lines each are then tapped by a 50-Ω feeding microstrip line at the center. The circuit is arranged symmetric with respect to the POS, whose intersection with the circuit-layout plane is denoted by the dashed line. For DM operation, the POS can be replaced by an electric

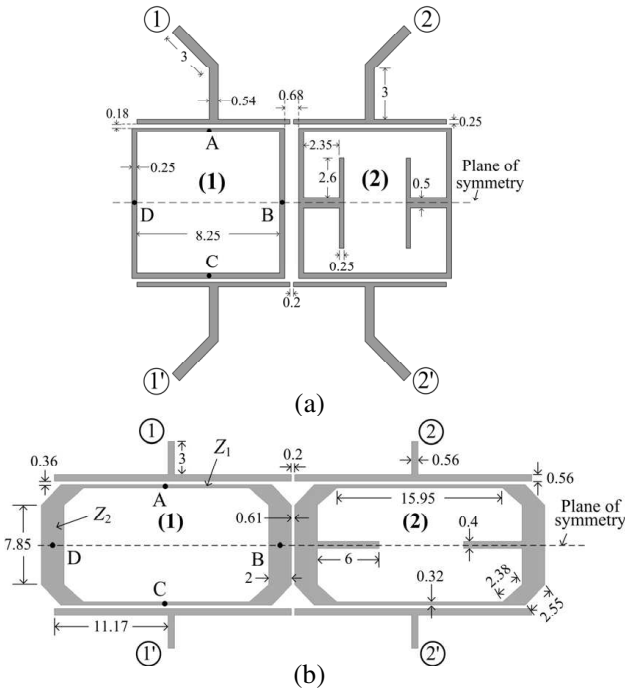

Figure 1. Configurations of the proposed balanced (a) single- and (b) dual-band BPFs.

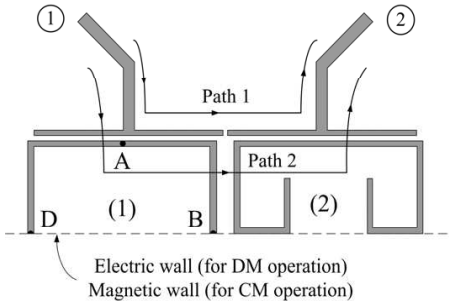

Figure 2. Equivalent half circuit of the single-band BPF.

wall, whereas for CM operation, by a magnetic wall. Hence, the portion of the circuit layout that connects to the POS can be regarded as grounded for DM operation and as open-circuited for CM operation. The original complete circuit can then be investigated by analyzing its corresponding two simpler half circuits shown in Fig. 2.

To understand why a DM signal can be transmitted in the desired frequency band and why a CM signal can be suppressed in the frequency range of interest, we first study the first few modal distributions of the voltage on the upper half ring resonator. For convenience, modal voltage distributions are plotted on the straightened version of the upper half of Resonator 1. The first three resonant modes for DM and CM operation are shown in Figs. 3(a) and 3(b), respectively. Since the two ends of the half ring resonator are grounded (open-circuited) for DM (CM) operation, the voltage is always zero (positive or negative maximum) at the two ends of the half ring resonator, i.e., at positions B and D. For convenience, refer to the half ring resonator in Fig. 3(a) as a short-circuited $\lambda/2$ resonator and the one in Fig. 3(b) as an open-circuited $\lambda/2$ resonator. Because the horizontal microstrip line above the $\lambda/2$ resonator is center-tapped, the voltage on the horizontal microstrip line is symmetrically distributed with respect to the tapping point. Also, since the voltages for the odd-numbered (even-numbered) modes of the short-circuited (open-circuited) $\lambda/2$ resonator are symmetrically distributed with respect to position A, Modes 1 and 3 of the short-circuited $\lambda/2$ resonator and Mode 2 of the open-circuited $\lambda/2$ resonator can easily be excited by the feeding line. On the other hand, since the voltages for the even-numbered (odd-numbered) modes of the short-circuited (open-circuited) $\lambda/2$ resonator are anti-symmetrically distributed, none of Mode 2 of the short-circuited $\lambda/2$ resonator and Modes 1 and 3 of the open-circuited $\lambda/2$ resonator can be excited provided the tapping point

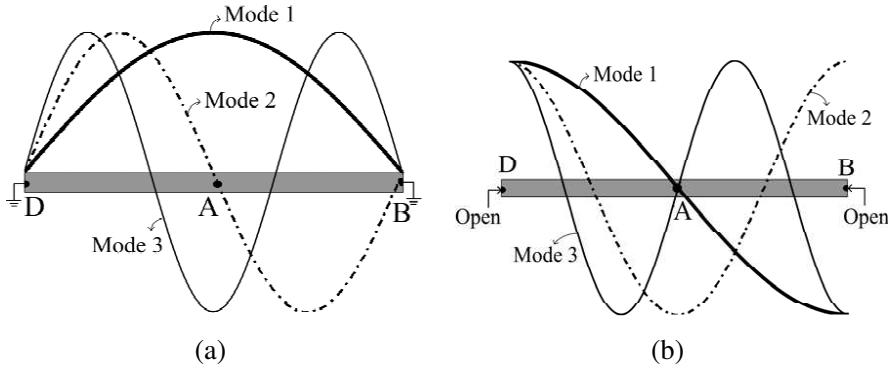

Figure 3. Voltage distributions on the straightened version of the $\lambda/2$ resonator shown in Fig. 2 for (a) DM and (b) CM operation.

of the horizontal microstrip line is aligned with position A, the center of the $\lambda/2$ resonator. For conciseness, let Mode n of the short-circuited (open-circuited) $\lambda/2$ resonator be called the nth differential (common) resonant mode.

For our balanced single-band BPF, the first differential resonant mode is designed around the center frequency of the desired DM passband, and the third differential resonant mode is considered as the first higher spurious DM mode. If Resonator 2 is merely a location-shifted version of Resonator 1, the second common resonant mode in Resonator 1 will in turn excite the same mode in Resonator 2, thus leading to an undesirable CM passband around the second CM resonant frequency. To prevent a CM signal from passing through Resonator 1 and then Resonator 2 via their second common resonant modes, two T-shaped open-circuited stubs are connected to Resonator 2 along the POS. With the open-circuited stubs of appropriate size added, the total length of the open-circuited $\lambda/2$ resonator associated with Resonator 2 is effectively increased [10, 13]. The resonant frequencies of the common resonant modes (or called the CM resonant frequencies for short) of Resonator 2 are hence lowered and deviates from those of Resonator 1. This results in poor CM transmissions. Furthermore, an even better CM rejection is expected around the first CM resonant frequencies of Resonators 1 and 2. This is not only because the first CM resonant frequencies of the two ring resonators are different, but also because the first common resonant mode of Resonator 2 still cannot be excited even though the associated open-circuited $\lambda/2$ resonator is lengthened by the open-circuited stubs. For DM operation, since the open-circuited stubs are connected to

the zero-potential points of Resonator 2, the associated DM resonant frequencies of Resonator 2 are not changed. Hence, the DM response of the proposed BPF can remain nearly unaltered in the presence of the open-circuited stubs.

For demonstration, the idea presented so far is employed to design a balanced BPF for 3.5-GHz WiMAX applications that require a frequency band of 3.39–3.6 GHz. The BPF is to be fabricated on a 0.635-mm-thick RT/Duroid 6010 substrate with $\varepsilon_r = 10.2$ and $\tan\delta = 0.0023$. The width of all microstrip sections in the BPF is chosen to be 0.25 mm except for the 50-Ω feeding microstrip lines, whose width is determined to be 0.54 mm. The fractional bandwidth Δ is selected to be 10%, which on the safe side is larger than the actually needed 6%. In addition, the second order Butterworth function is used as the target BPF response for which the element values for the low-pass prototype network are $g_0 = g_3 = 1$ and $g_1 = g_2 = \sqrt{2}$. Hence, the required coupling coefficient between Resonators 1 and 2 for DM operation at 3.5 GHz is $M = \Delta/\sqrt{g_1 g_2} = 0.0707$, which is found to correspond to a gap of 0.68 mm between the two resonators after parametric studies are carried out [26]. Note that the selectivity of the Butterworth response can be enhanced by implanting a transmission zero near each of the passband edges. This can be accomplished by forming a cross-coupled structure for which its two signal paths are indicated in Fig. 2. In this figure, path 1 is the source-load coupling path established by reducing the gaps between the juxtaposed horizontal microstrip lines that are tapped by the feeding lines, and path 2 is the route passing through Resonators 1 and 2. With the aid of the commercial full-wave simulator Ansoft HFSS, which is convenient to electromagnetically characterize a three-dimensional object, the structural parameters can be determined as those indicated in Fig. 1(a) with all units in millimeter.

2.2. Results and Discussion

With the structural parameters available, we are now ready to verify that the well-adjusted cross-coupling configuration can produce a transmission zero near each of the two DM passband edges. The two transmission zeros are due to cancellation of the signals transmitted along paths 1 and 2. Note that if a full-wave simulator is employed, signals transmitted along these two paths cannot be isolated (i.e., cannot be separately computed). We hence resort to Agilent's Advanced Design System (Agilent ADS) for that purpose. In using this software, the half circuit in Fig. 2 is substituted by equivalent circuit models that can account for parallel coupling, bending, and junction. In simulating the frequency response of path 1, the vertical

parallel-coupled line section is replaced by two uncoupled line sections in the circuit schematic. Likewise, in the frequency-response simulation for path 2, the gap-coupling model for the two juxtaposed horizontal center-tapped microstrip lines is eliminated from the circuit schematic. Fig. 4 shows the DM transmission response for three cases: path 1 only, path 2 only, and the overall half circuit. Also shown in Fig. 4 is the phase difference between paths 2 and 1. Clearly, the transmission zeros may occur at the frequencies such that the signals transmitted along these two paths have nearly the same magnitude and a phase difference of roughly odd multiples of 180°. Note that there is also a transmission zero for path 1 alone around 3.5 GHz. At this frequency, which is the first resonant frequency of the short-circuited $\lambda/2$ resonator, the input signal is not transmitted to the output along path 1 but instead is trapped by the short-circuited $\lambda/2$ resonator.

For completeness, we next employ Ansoft HFSS to verify that the open-circuited stubs can effectively lower the CM resonant frequencies of the ring resonator while little affecting the DM counterparts. For convenience, the ring resonator is chosen to be loaded by horizontal straight open-circuited stubs instead of the T-shaped stubs shown in Fig. 1(a). In addition, the structural dimensions of the ring resonator and the width of the horizontal open-circuited stubs are chosen the same as those in Fig. 1(a). Presented in Fig. 5 are the first two DM and CM resonant frequencies against the length (L) of the open-circuited stubs (see the inset, in which only the half circuit is shown). Clearly, with L increased from 0 to 3.8 mm, the CM resonant frequencies are significantly lowered while the DM counterparts are almost independent of L. The decrease in the second CM resonant frequency is more pronounced than in the first. This is because the same physical length L corresponds to a larger electric length for the

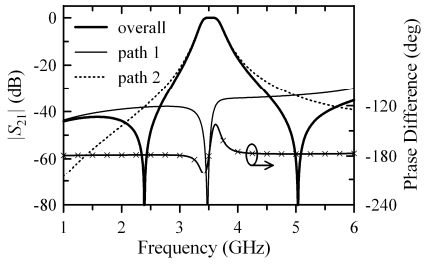

Figure 4. DM transmission response of the BPF simulated using commercial Agilent ADS.

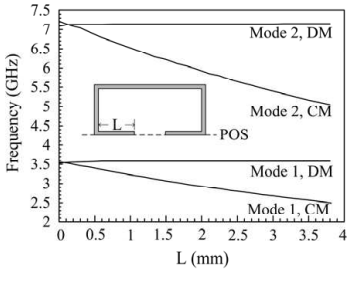

Figure 5. Influence of the open-stub length on mode frequencies of the ring resonator.

second CM resonant mode than for the first.

Figure 6 shows the photograph of the fabricated balanced single-band BPF, which when excluding the 50-Ω feeding microstrip lines measures only $18.2 \times 9.7\,\text{mm}^2$. The feeding microstrip lines are bent by 45° to provide enough space for installing SMA connectors. Simulated and measured S-parameters are shown in Fig. 7(a) for DM operation and in Fig. 7(b) for CM operation. The measurement agrees reasonably well with the simulation. For the DM response, the measured (simulated) passband of 3.35–3.65 (3.34–3.65) GHz with a center frequency of 3.495 (3.49) GHz has a minimum insertion loss of 1.4 (1.1) dB and a return loss of as high as 18.4 (22.7) dB. The measured and full-wave-simulated transmission zeros are very close to each other and are found to be around 2.25 and 4.94 GHz, which are slightly different from the circuit-model-simulated transmission zeros of 2.39 and 5.04 GHz (see Fig. 4). These discrepancies could be attributed to the fact that the electric wall on the POS and mutual couplings between circuit subcomponents cannot be accounted for in circuit-model simulation. The transmission zeros owing to the cross-coupling configuration are effective in suppressing out-of-band signals. In the frequency range of 1–8 GHz, the out-of-band rejection is larger than 30 dB except for the passband edges and the frequency range of around 7.1 GHz, which is roughly the second DM resonant frequency. As claimed previously, the second differential resonant modes for both resonators are not supposed to be excited in the initial design stage. However, because the end-coupled horizontal center-tapped microstrip lines are brought slightly closer to establish the source-load coupling, the condition of not exciting the even-numbered differential resonant modes is violated (i.e., the tapping point of the horizontal microstrip line is not aligned with position A of the $\lambda/2$ resonator) Hence, the even-numbered differential resonant modes are instead weakly excited. This explains why the out-of-band rejection around 7.1 GHz is slightly downgraded.

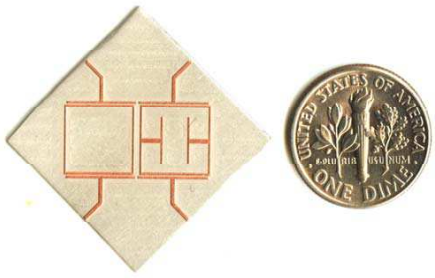

Figure 6. Photograph of the balanced single-band BPF.

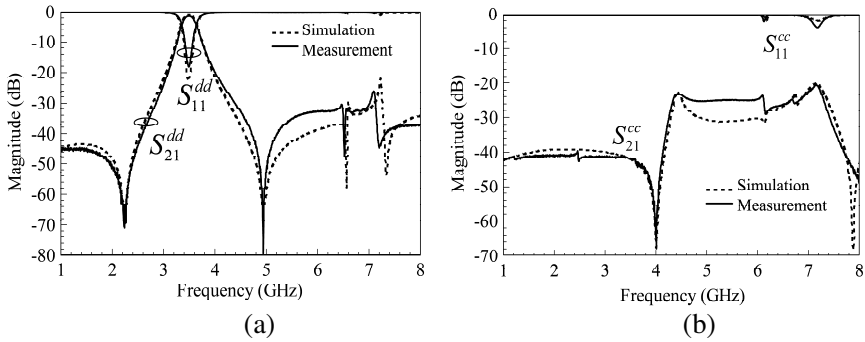

Figure 7. Simulated and measured S-parameter for the fabricated balanced single-band BPF.

For the CM response in 1–8 GHz, although the measured (simulated) minimum insertion loss is only 20.7 (20.1) dB around 7.15 GHz, which is around the second CM resonant frequency of Resonator 1, it is larger than 41.6 (41.3) dB in the DM passband. Note that the full-wave-simulated CM transmission zeros around 4 and 7.9 GHz are also due to the cross-coupling configuration. If evaluated by using circuit-model simulation, the CM transmission zeros will be around 4.24 and 8.63 GHz. These discrepancies could be due to lack of the magnetic wall and lack of inter-subcomponent mutual couplings in circuit-model simulation.

An alternative set of indicators of how well a balanced BPF performs are the amplitude and phase imbalances. A signal enters a single port, say port 1, can be decomposed into a DM and a CM component. The amplitude and phase imbalances can then be defined by $||S_{21}| - |S_{2'1}||$ and $\angle S_{21} - \angle S_{2'1}$, respectively. An ideal balanced BPF in the DM passpand will transmit only the DM component and completely reject the CM component, thus leading to an amplitude imbalance of 0 dB and a phase imbalance of 180°. Not shown in a figure for brevity, the measured amplitude and phase imbalances for the fabricated balanced single-band BPF in the DM passband are found to be 0.07–0.29 dB and 177.15°–182.25°, respectively, which are close to the ideal values.

3. DESIGN OF BALANCED DUAL-BAND BPF

3.1. BPF Configuration and Design

Figure 1(b) shows the proposed ring-type balanced dual-band BPF. In contrast to the proposed single-band BPF where the rings are of

uniform impedance, the dual-band BPF adopts stepped-impedance ring resonators (SIRRs; the one on the left side is referred to as SIRR 1, and that on the right, SIRR 2). Other than that, all the concepts behind the design of the single-band BPF are employed here to design the dual-band one. For example, the BPF circuit layout is arranged symmetric with respect to the POS (see Fig. 1(b)) so that none of the DM-to-CM and CM-to-DM conversions can occur. Next, the SIRRs and the center-tapped horizontal microstrip lines in the initial design stage are deployed in such a way that none of the even-numbered differential and odd-numbered common resonant modes can be excited by the feeding microstrip lines. In addition, two open-circuited stubs are connected to SIRR 2 along the POS, so that the CM resonant frequencies of SIRR 2 are shifted away from those of SIRR 1. As a result, an even-numbered common resonant mode excited on one SIRR by its feeding lines will not in turn excite the corresponding common resonant mode on the other SIRR, thus leading to CM rejection. Last, the juxtaposed horizontal microstrip lines are brought closer to establish the source-load coupling. The resulting additional signal transmission path can help create transmission zeros near the edges of the two desired DM passbands.

For demonstration, the balanced dual-band BPF is designed for use in the popular 2.4-GHz (2.4–2.484 GHz) and 5.2-GHz (5.15–5.35 GHz) WLAN bands and is fabricated on the same RT/Duroid 6010 substrate as the one adopted for the single-band BPF. In Fig. 1(b), let the microstrip of from positions D to A and then to B be referred to as a $\lambda/2$ stepped-impedance resonator, or $\lambda/2$ SIR for short. In this $\lambda/2$ SIR, let the characteristic impedance of the center microstrip section (i.e., the section covering position A) be denoted by Z_1, and that of the two end sections (i.e., the sections associated with positions D and B), Z_2. In addition, the section with Z_1 in the $\lambda/2$ SIR has an electric length of $2\theta_1$, and each of the sections with Z_2, θ_2. To make the design easier, we proceed with the assumption that $\theta_1 = \theta_2 = \theta_0$ since under this constraint the impedance ratio R_Z, which is equal to Z_2/Z_1, can be determined analytically from the given resonant frequencies of the $\lambda/2$ SIR [27]. With f_1 and f_3 denoting the desired odd-numbered DM resonant frequencies, which of course are set to be the center frequencies of the desired lower and upper DM passbands, respectively, the impedance ratio can be calculated by

$$\theta_0 (f_1) = \cot^{-1}\sqrt{R_z} = \pi/(1 + f_3/f_1) \tag{1}$$

Note that this equation is slightly different from that given in [27] because the two ends of the $\lambda/2$ SIR in our DM operation are short-circuited rather than open-circuited as in [27]. By setting f_1 and f_3 to be 2.45 and 5.25 GHz, respectively, we can find that $R_Z = 0.413$ and

$\theta_0(f_1) = 57.27°$. To proceed with convenience, we fix Z_2 at 24.4 Ω so that the corresponding line width of 2 mm is an integer value. All other relevant structural parameters can in turn be computed accordingly. In fact, these structural parameters still need to undergo fine tuning in deploying the entire BPF because the effects of dispersion and the mitered bending discontinuities are not taken into account in Eq. (1). The BPF's structural parameters, optimized also with the aid of Ansoft HFSS, are given in Fig. 1(b).

3.2. Results and Discussion

Figure 8 shows the photograph of the fabricated balanced dual-band BPF, which when exclusive of the 50-Ω feeding lines occupies an area of $46.2 \times 13.8\,\text{mm}^2$. As shown in Fig. 9, the simulated and measured S-parameters agree well to each other. For the DM response, the measured (simulated) first and second passbands of 2.39–2.49 (2.4–2.5) and 5.15–5.35 (5.15–5.36) GHz, respectively, are centered at 2.44 (2.45) and 5.25 (5.25) GHz and have minimum insertion losses of 1 (1.3) and 1.3 (1.5) dB. The out-of-band rejection is larger than 20 dB except for the frequency range of around 4 GHz, within which the second

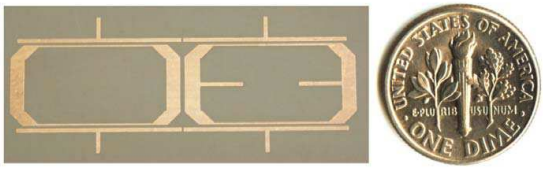

Figure 8. Photograph of the balanced dual-band BPF.

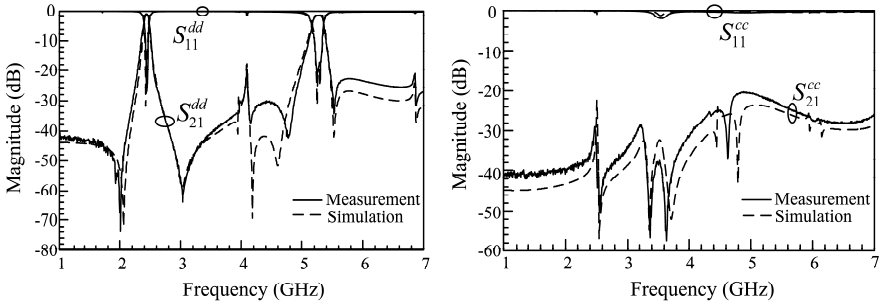

Figure 9. Simulated and measured S-parameters for the fabricated balanced dual-band BPF.

differential resonant mode appears not completely suppressed because of the source-load coupling. For the CM response in the displayed frequency range of 1–7 GHz, the measured (simulated) insertion loss is greater than 20.5 (22) dB. In particular, the measured CM suppressions in the first and second DM passbands are larger than 29 and 22 dB, respectively.

4. CONCLUSION

In this paper, ring resonators have been proposed to be used as the building blocks of two balanced BPFs, one single-banded and the other dual-banded. Source-load couplings were established in both BPF prototypes so that two DM transmission zeros are generated around the two edges of each passband to sharpen the DM passband selectivity. For design of both BPFs, a technique of loading a pair of open-circuited stubs along the POS of one of the coupled SIRRs for separating the CM resonant frequencies has been employed, and very good CM suppression was obtained.

ACKNOWLEDGMENT

This work was supported by the National Science Council of the Republic of China (in Taiwan) under Grant NSC 98-2221-E-018-005.

REFERENCES

1. Razavi, B., *Design of Analog CMOS Integrated Circuits*, 101–102, McGraw-Hill, 2001.
2. Wu, C. H., C. H. Wang, and C. H. Chen, "Novel balanced coupled-line bandpass filters with common-mode noise suppression," *IEEE Trans. Microwave Theory Tech.* Vol. 55, No. 2, 287–295, Feb. 2007.
3. Lee, C.-H., I.-C. Wang, and C.-I. G. Hsu, "Balanced dual-band BPF using $\lambda/4$ stepped-impedance resonators and folded feed lines," *Journal of Electromagnetic Wave and Applications*, Vol. 23, No. 17–18, 2441–2449, 2009.
4. Lim, T. B. and L. Zhu, "A differential-mode wideband bandpass filter on microstrip line for UWB application," *IEEE Microw. Wireless Compon. Lett.*, Vol. 19, No. 10, 632–634, Oct. 2009.
5. Lim, T. B. and L. Zhu, "Differential-mode ultra-wideband bandpass filter on microstrip line," *Electronics Lett.*, Vol. 45, No. 22, 1124–1125, Oct. 2009.

6. Wu, C. H., C. H. Wang, and C. H. Chen, "Stopband-extended balanced bandpass filter using coupled stepped-impedance resonators," *IEEE Microw. Wireless Compon. Lett.*, Vol. 17, No. 7, 507–509, Jul. 2007.
7. Wu, C. H., C. H. Wang, and C. S. H. Chen, "Balanced coupled-resonator bandpass filters using multisection resonators for common-mode suppression and stopband extension," *IEEE Trans. Microwave Theory Tech.*, Vol. 55, No. 8, 1756–1763, Aug. 2007.
8. Chen, X., G. Han, R. Ma, J. Gao, and W. Zhang, "Design of balanced dual-band Bandpass Filter with self-feedback structure," *ETRI Journal*, Vol. 31, No. 3., 475–477, Aug. 2009.
9. Lee, C.-H., C.-I. G. Hsu, and C.-C. Hsu, "Balanced dual-band BPF with stub-loaded SIRs for common-mode suppression," *IEEE Microw Wireless Compon. Lett.*, Vol. 17, No. 2, 70–72, Feb. 2010.
10. Hsu, C.-I. G., C.-C. Hsu, C.-H. Lee, and H.-H. Chen, "Balanced dual-band BPF using only equal-electric-length SIRs for common-mode suppression," *Journal of Electromagnetic Waves and Applications*, Vol. 24, No. 5–6, 695–705, 2010
11. Shi, J. and Q. Xue, "Novel balanced dual-band bandpass filter using coupled stepped-impedance resonators," *IEEE Microw. Wireless Compon. Lett.*, Vol. 20, No. 1, 19–21, Jan. 2010.
12. Shi, J. and Q. Xue, "Balanced bandpass filters using center-loaded half-wavelength resonators," *IEEE Trans. Microw. Theory Tech.*, Vol. 58, No. 4, 970–977, Apr. 2010.
13. Zhang, X. Y., J.-X. Chen, Q. Xue, and S.-M. Li, "Dual-band bandpass filter using stub-loaded resonators," *IEEE Microw. Wireless Compon. Lett.*, Vol. 17, No. 8, 583–585, Aug. 2007.
14. Garmjani, N. M. and N. Komjani, "Quasi-elliptic bandpass filter based on SIR with elimination of first spurious response," *Progress In Electromagnetics Research C*, Vol. 9, 89–100, 2009.
15. Hsu, C.-I. G., C.-H. Lee, and Y.-H. Hsieh, "Tri-band bandpass filter with sharp passband skirts designed using tri-section SIRs," *IEEE Microw. Wireless Compon. Lett.*, Vol. 18, No. 1, 19–21, Jan. 2008.
16. Chin, K.-S. and C.-K. Lung, "Miniaturized microstrip dual-band bandstop filters using tri-section stepped-impedance resonators," *Progress In Electromagnetics Research C*, Vol. 10, 37–48, 2009.
17. Lin, W.-J., C.-S. Chang, J.-Y. Li, D.-B. Lin, L.-S. Chen, and M.-P. Houng, "A new approach of dual-band filters by stepped impedance simplified cascaded quadruplet resonators with slot

coupling," *Progress In Electromagnetics Research Letters*, Vol. 9, 19–28, 2009.

18. Chang, K. and L.-H. Hsieh, *Microwave Ring Circuits and Related Structures*, 2nd edition, John Wiley and Sons, 2004.
19. Zhao, L.-P., X.-W. Dai, Z.-X. Chen, and C.-H. Liang, "Novel design of dual-mode dual-band bandpass filter with triangular Resonators," *Progress In Electromagnetics Research*, Vol. 77, 417–424, 2007.
20. Wu, G.-L., W. Mu, X.-W. Dai, and Y.-C. Jiao, "Design of novel dual-band bandpass filter with microstrip meander-loop resonator and CSRR DGS," *Progress In Electromagnetics Research*, Vol. 78, 17–24, 2008.
21. Esfeh, B. K., A. Ismail, R. S. A. Raja Abdullah, H. Adam, and A. R. H. Alhawari, "Compact narrowband bandpass filter using dual-mode octagonal meandered loop resonator for Wimax application," *Progress In Electromagnetics Research B*, Vol. 16, 277–290, 2009.
22. Al-Zayed, A. S. and S. F. Mahmoud, "On the design of an improved dual operation wide band ring resonator filter," *Journal of Electromagnetic Waves and Applications*, Vol. 23, No. 14–15, 1939–1946, 2009.
23. Mo, S.-G., Z.-Y. Yu, and L. Zhang, "Design of triple-mode bandpass filter using improved hexagonal loop resonator, *Progress In Electromagnetics Research*, Vol. 96, 117–125, 2009.
24. Lin, H.-J., X.-W. Shi, X. H. Wang, C.-L. Li, and Q. Li, "A novel CPW dual passband filter using the split-modes of loaded stub square loop resonators," *Progress In Electromagnetics Research Letters*, Vol. 16, 45–52, 2010.
25. Yang, R. Y., Y. L. Lin, and C. Y. Hung, "A modified dual-mode ultra-wideband band-pass filter fabricated on ultra thin liquid crystal polymer substrate," *Journal of Electromagnetic Waves and Applications*, Vol. 24, No. 10, 1397–1404, 2010.
26. Hong, J.-S. and M. J. Lancaster, *Microstrip Filters for RF/Microwave Application*, John Wiley and Sons, 2001.
27. Makimoto, M. and S. Yamashita, "Bandpass filters using parallel coupled stripline stepped impedance resonators," *IEEE Trans. Microwave Theory Tech.*, Vol. 28, No. 12, 1413–1417, Dec. 1980.